Heterospin complexes of fluorinated dinuclear Cu^{II} and Mn^{II} triketonates with nitroxides*

V. I. Ovcharenko,[a]★ S. V. Fokin,[a] G. V. Romanenko,[a] A. S. Bogomyakov,[a] D. S. Yachevskii,[b] D. L. Chizhov,[b] V. N. Charushin,[b]★ and O. N. Chupakhin[b]

[a] *International Tomography Center, Siberian Branch of the Russian Academy of Sciences, 3a ul. Institutskaya, 630090 Novosibirsk, Russian Federation. Fax: +7 (383) 333 1399. E-mail: Victor.Ovcharenko@tomo.nsc.ru*

[b] *I. Ya. Postovsky Institute of Organic Synthesis, Ural Branch of the Russian Academy of Sciences, 22 ul. S. Kovalevskoi, 620041 Ekaterinburg, Russian Federation. Fax: +7 (343) 369 3058. E-mail: charushin@ios.uran.ru*

Dinuclear heterospin complexes of Cu^{II} and Mn^{II} 1,1,1,7,7,7-hexafluoroheptane-2,4,6-trionates ($[Cu_2L_2]$ and $[Mn_2L_2]$, respectively) with nitronyl nitroxides 2-R-4,4,5,5-tetramethyl-4,5-dihydro-1*H*-imidazole-3-oxide 1-oxyls (NIT—R, R = H, Me, Et, *m*-C_5H_4N, *m*-NCC_6H_4, *p*-NCC_6H_4, PzMe) and the diradical NIT—Pz—$(CH_2)_4$—Pz—NIT (Pz is 1,4-pyrazolylene) were synthesized and structurally characterized. In the complexes under study, the Cu^{II} atom tends to have the square-pyramidal coordination environment, and the Mn^{II} atom is in an octahedral environment. The magnetochemical investigation of the compounds in the temperature range of 2—300 K showed that the antiferromagnetic exchange coupling dominates in the $[Cu_2L_2]$ molecules, whereas this coupling in $[Mn_2L_2]$ is manifested in the experimental plot $\mu_{eff}(T)$ at $T < 100$ K. The magnetic properties of the heterospin complexes of $[Cu_2L_2]$ with NIT—R are also determined by the intramatrix antiferromagnetic exchange coupling. For the complexes of $[Mn_2L_2]$ with NIT—R, the coordination mode of the nitroxide plays a decisive role.

Key words: copper(II), manganese(II), metal triketonates, nitroxides, X-ray diffraction study, magnetic properties.

Fluorinated chelates are widely used as acceptor matrices in the synthesis of heterospin systems containing nitroxides.[1,2] The high accepting ability of metal ions incorporated into such matrices is favorable for the coordination of weak donors (nitroxyl groups of nitroxides) resulting in the formation of heterospin exchange clusters. Among compounds based on copper(II) bis(hexafluoroacetylacetonate) ($Cu(hfac)_2$) with nitronyl nitroxides (NIT—R) containing such heterospin exchange clusters, there is an unusual family of heterospin complexes characterized by thermally induced magnetic effects, whose temperature dependences of the effective magnetic moment are analogous to those of the spin-crossover.[3—14] These complexes show a strong temperature dependence of the exchange integral determined by the structural dynamics of the exchange cluster in the magnetic anomaly region[15,16] and can exhibit a LIESST effect, which can be detected with the use of an original procedure based on ESR spectroscopy.[17]

The discovery of these new magnetically active systems has called for a detailed study of the structures and magnetic properties of these heterospin complexes, which made it necessary to extend the range of such compounds. It should be noted that the systematic studies of this type of compounds are based primarily on the successive variation of the substituent R in nitronyl nitroxide molecules and the preparation of solid solutions containing either various paramagnetic organic ligands or different metals in the matrix $M(hfac)_2$.[3,4] A fluorinated metal-containing matrix is in itself varied in rare cases. Only recently,[18] molecular complexes of bis(μ_2-1,1,2,2,8,8,9,9-octafluorononane-3,5,7-trionato)dicopper(II) ($[Cu_2L'_2]$) with NIT—PzMe (Pz is 1,4-pyrazolylene) and NIT—*m*-C_5H_4N have been synthesized and characterized. In this connection, we made an attempt to synthesize heterospin complexes based on NIT—R and the dinuclear fluorinated matrices bis(μ_2-1,1,1,7,7,7-hexafluoroheptane-2,4,6-trionates)dicopper(II) ($[Cu_2L_2]$) and -dimanganese(II) ($[Mn_2L_2]$). We used mainly NIT—R as nitroxides. These compounds react with $[Cu(hfac)_2]$ to form complexes exhibiting thermally induced magnetic anomalies.[3,4,16] In the

* Dedicated to Academician of the Russian Academy of Sciences I. L. Eremenko on the occasion of his 60th birthday.

Published in Russian in *Izvestiya Akademii Nauk. Seriya Khimicheskaya,* No. 6, pp. 1138—1149, June, 2010.

1066-5285/10/5906-1162

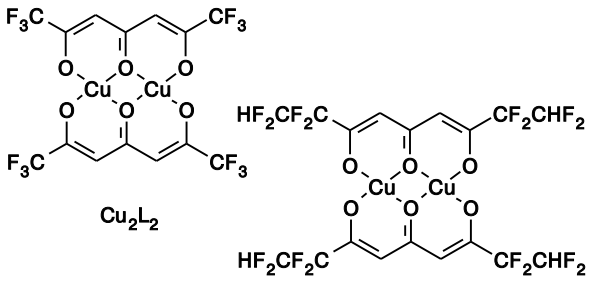

Cu_2L_2

$Cu_2L'_2$

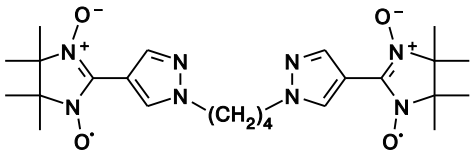

NIT—Pz—$(CH_2)_4$—Pz—NIT

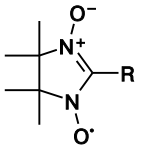

NIT—R

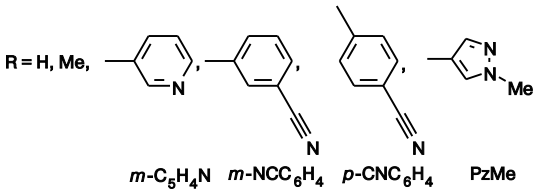

R = H, Me, *m*-C_5H_4N *m*-NCC_6H_4 *p*-CNC_6H_4 PzMe

present study, we discuss the characteristic features of the synthesis, the structures of the complexes $[Cu_2L_2]\cdot 2C_7H_8$ (**1**), $[Cu_2L_2(NIT—PzMe)_2]$ (**2**), $[Cu_2L_2(NIT—PzMe)_2]\cdot Me_2CO\cdot C_7H_8$ (**2**$\cdot Me_2CO\cdot C_7H_8$), $[Cu_2L_2(NIT—m\text{-}C_5H_4N)_2]\cdot CH_2Cl_2$ (**3**$\cdot CH_2Cl_2$), $[(Cu_2L_2)_2(NIT—Pz—(CH_2)_4—Pz—NIT)_3]\cdot 3C_7H_8$ (**4**$\cdot 3C_7H_8$), $\{[(Cu_2L_2)_2(NIT—Pz\text{-}(CH_2)_4—Pz—NIT)_3][Cu_2L_2(EtOH)_4]\}\cdot C_7H_8$ (**5**$\cdot C_7H_8$), $[Cu_2L_2(NIT—p\text{-}NCC_6H_4)]$ (**6**), $[Cu_2L_2(NIT—p\text{-}NCC_6H_4)_2(EtOH)_2]$ (**7**), $[Cu_2L_2(NIT—m\text{-}NCC_6H_4)_2]$ (**8**), $[Cu_2L_2(EtOH)_2]\cdot NIT—m\text{-}NCC_6H_4$ (**9**), $[Cu_2L_2(NIT—Me)_2]$ (**10**), $[Cu_2L_2(NIT—Me)]$ (**11**), $[Mn_2L_2(NIT—H)_4]$ (**12**), $[Mn_2L_2(NIT—Me)_4]\cdot EtOH$ (**13**$\cdot$EtOH), $[Mn_2L_2(NIT—Me)_2]$ (**14**), $[Mn_2L_2(NIT—Et)_2]$ (**15**), and $[Mn_2L_2(NIT—m\text{-}NCC_6H_4)_2(H_2O)_2]\cdot 2(NIT—m\text{-}NCC_6H_4)$ (**16**), and the temperature dependences of the effective magnetic moment for these complexes.

Results and Discussion

Synthesis. Procedures for the synthesis described in the Experimental section allow the preparation of coordination compounds as single crystals suitable for X-ray diffraction study. The choice of the solvents and their mixtures for the synthesis of dinuclear heterospin complexes with NIT—R was determined by the possibility of the preparation of compounds as single crystals. In principle, the dinuclear complexes of $[Cu_2L_2]$ with NIT—R can be isolated from different solvents. For example, the complexes with NIT—PzMe and NIT—*m*-C_5H_4N can be synthesized in diethyl ether, acetone, toluene, or CH_2Cl_2.

It should be noted that the solubility of the dinuclear complex $[Cu_2L_2]$ and its complexes with nitroxides in organic solvents is substantially lower than that of the mononuclear complex $Cu(hfac)_2$ and its complexes with the corresponding nitroxides. In terms of the kinetic stability in solution, the dinuclear complexes of $[Cu_2L_2]$ with NIT—R are much less reactive that the related complexes of $Cu(hfac)_2$. The $[Cu_2L_2]$: NIT—R ratio may be of importance in the synthesis of the complexes. For example, under the same conditions, NIT—Me gives $[Cu_2L_2(NIT—Me)]$ (**11**) or $[Cu_2L_2(NIT—Me)_2]$ (**10**) as the solid phase depending on the ratio $[Cu_2L_2]$: NIT—Me (1 : 1 or 1 : 2, respectively). By contrast, complexes in which NIT—R contain stronger donor atoms compared to the >N—O group have the stoichiometry 1 : 2 regardless of the starting ratio of the reagents in solution. On the one hand, this is indicative of their individual state. However, on the other hand, this strongly reduces the diversity of possible heterospin compounds.

The structure of the resulting molecule is substantially influenced by the nature of the ligand. Thus, both ligands in the complex with NIT—PzMe are coordinated on the same side of the $[Cu_2L_2]$ plane. Variations of the conditions of the synthesis, as well as the use of other solvents, the diradical analog, and the related matrix $[Cu_2L'_2]$,[18] always led to compounds with this coordination mode for both nitroxide molecules (*cf.* Fig. 1, Fig. 2, *a*, and Fig. 3). The factors responsible for this coordination remain unclear and call for a special investigation. At least, this coordination mode was not observed in the other compounds under study. Moreover, the use of 4-iodo-1-methylpyrazole (I—PzMe) in the reaction with $[Cu_2L_2]$ leads to the formation of $[Cu_2L_2(I—PzMe)_2]$ in nearly quantitative yield. In the latter compound, the diamagnetic I—PzMe ligands are on the opposite sides of the coordination plane $[Cu_2L_2]$ (Fig. 2, *c*).

Structure. It should be noted that the structural data for transition metal complexes with L are scarce. Only the complex with methanol $[Cu_2L_2(MeOH)_2]$[19] was found in the Cambridge Structural Database. In the cited study, the synthesis of $[Cu_2L_2(H_2O)_2]$ was also described, but the structure of the latter compound was not determined.

The dinuclear matrix $[Cu_2L_2]$ without additional coordinated ligands was isolated as the solvate of the composition $[Cu_2L_2]\cdot 2C_7H_8$ (**1**) by crystallization from toluene (see Fig. 1, *a*). Both crystallographically independent

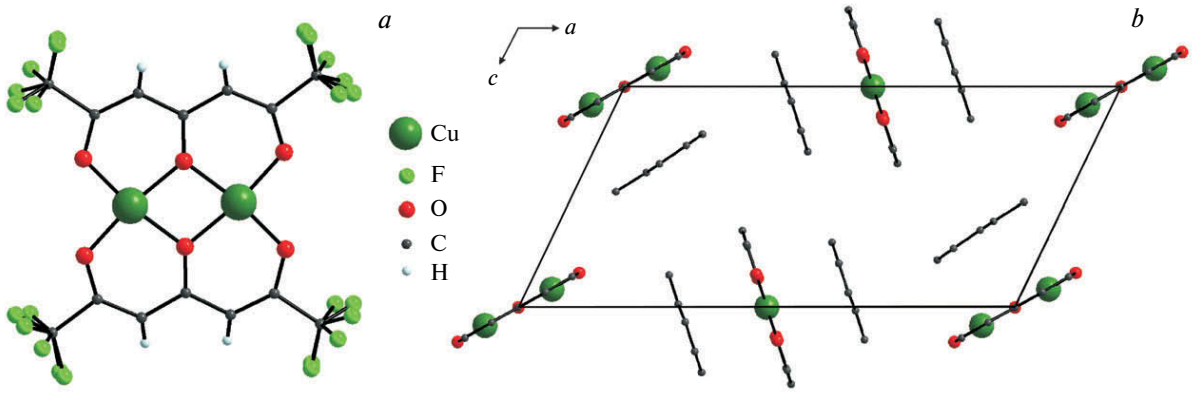

Fig. 1. Molecular structure of Cu_2L_2 (*a*) and a fragment of the crystal packing of $[Cu_2L_2]\cdot 2C_7H_8$ (**1**) (*b*, the H atoms and the Me groups are not shown).*

molecules are virtually planar; the deviations of the atoms from the mean plane passing through all atoms (except for H and F atoms) are at most 0.04 Å. The Cu—O distances to the terminal O atoms (1.874(2) and 1.878(3) Å) are substantially shorter than the corresponding distances to the bridging O atoms (1.927(2) and 1.922(2) Å). It should be noted that this ratio between the $Cu—O_{term}$ and $Cu—O_{bridg}$ distances is retained in all the complexes based on this matrix (Table 1). The $CuO_{bridg}Cu$ angles are 102.3(1) and 102.8(1)°; the intramatrix Cu...Cu distance is 3.001(1) Å. Figure 1, *b* shows the packing mode of the $[Cu_2L_2]$ and toluene molecules in the solid phase.

As in the case of the matrix $[Cu_2L'_2]$, nitroxides in the molecules $[Cu_2L_2(NIT—PzMe)_2]\cdot Me_2CO\cdot C_7H_8$ and $[Cu_2L_2(NIT—m\text{-}C_5H_4N)_2]$ (Fig. 2, *a*, *b*) are in different coordination with respect to the plane of the dinuclear matrix. The square pyramidal coordination of the Cu atom causes its displacement from the plane of the base toward the apex by ~0.25 Å. The N—O bond lengths in NIT—R are in the range of 1.263(6)—1.274(4) Å and are typical of nitroxides. The bond lengths and the MON angles in the coordination units of all complexes, as well as the N—O bond lengths in the nitroxides, are given in Table 1.

The coordination of nitroxide on one side of the plane of the chelate matrix is characteristic of $[Cu_2L'_2(NIT—PzMe)_2]$[18] and $[Cu_2L_2(NIT—PzMe)_2]$ (**2**) and is retained in the compounds containing the pyrazole moiety in the diradical (Fig. 3). The reaction of the diradical $NIT—Pz—(CH_2)_4—Pz—NIT$ with $[Cu_2L_2]$ affords the solid two-matrix tetranuclear heterospin complex $[(Cu_2L_2)_2(NIT—Pz—(CH_2)_4—Pz—NIT)_3]\cdot 3C_7H_8$ (**4**$\cdot 3C_7H_8$) with three diradical molecules. It is interesting that the recrystallization of this complex from EtOH is accompanied by the partial decomposition of the molecules to give the dinuclear complexes $[Cu_2L_2(EtOH)_4]$. These complexes link the former two-matrix molecules $[(Cu_2L_2)_2(NIT—Pz—(CH_2)_4—Pz—NIT)_3]$ to form chains through hydrogen bonds between the OH groups of the coordinated EtOH molecules and the O atoms of >N—O groups (see Fig. 3, *b*). It should be noted that there are

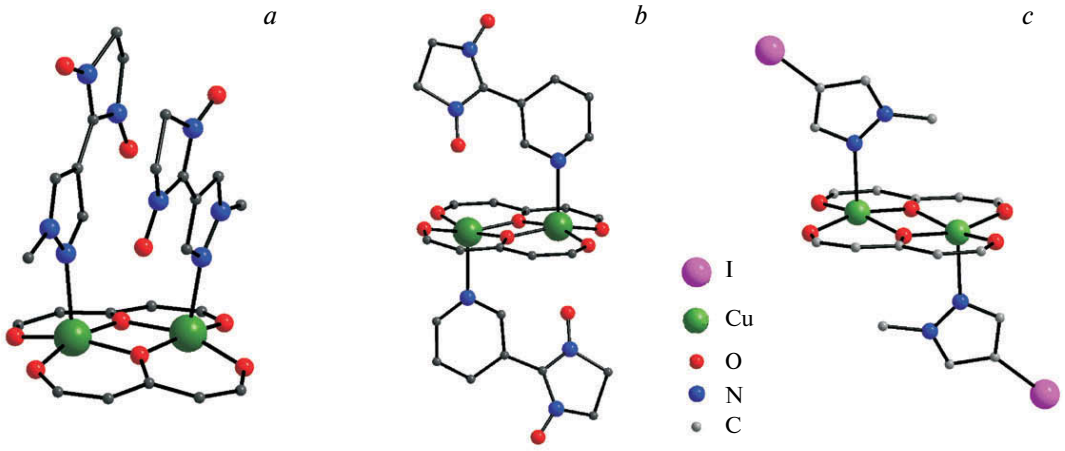

Fig. 2. Structures of the dinuclear molecules in $[Cu_2L_2(NIT—PzMe)_2]$ (**2**) (*a*), $[Cu_2L_2(NIT—m\text{-}C_5H_4N)_2]$ (**3**) (*b*), and $[Cu_2L_2(I\text{-}PzMe)_2]$ (*c*). The H atoms and the Me and CF_3 groups are not shown in Figs 2—9.

* Figures 1—9 are available in full color in the on-line version of the journal (http://www.springerlink.com).

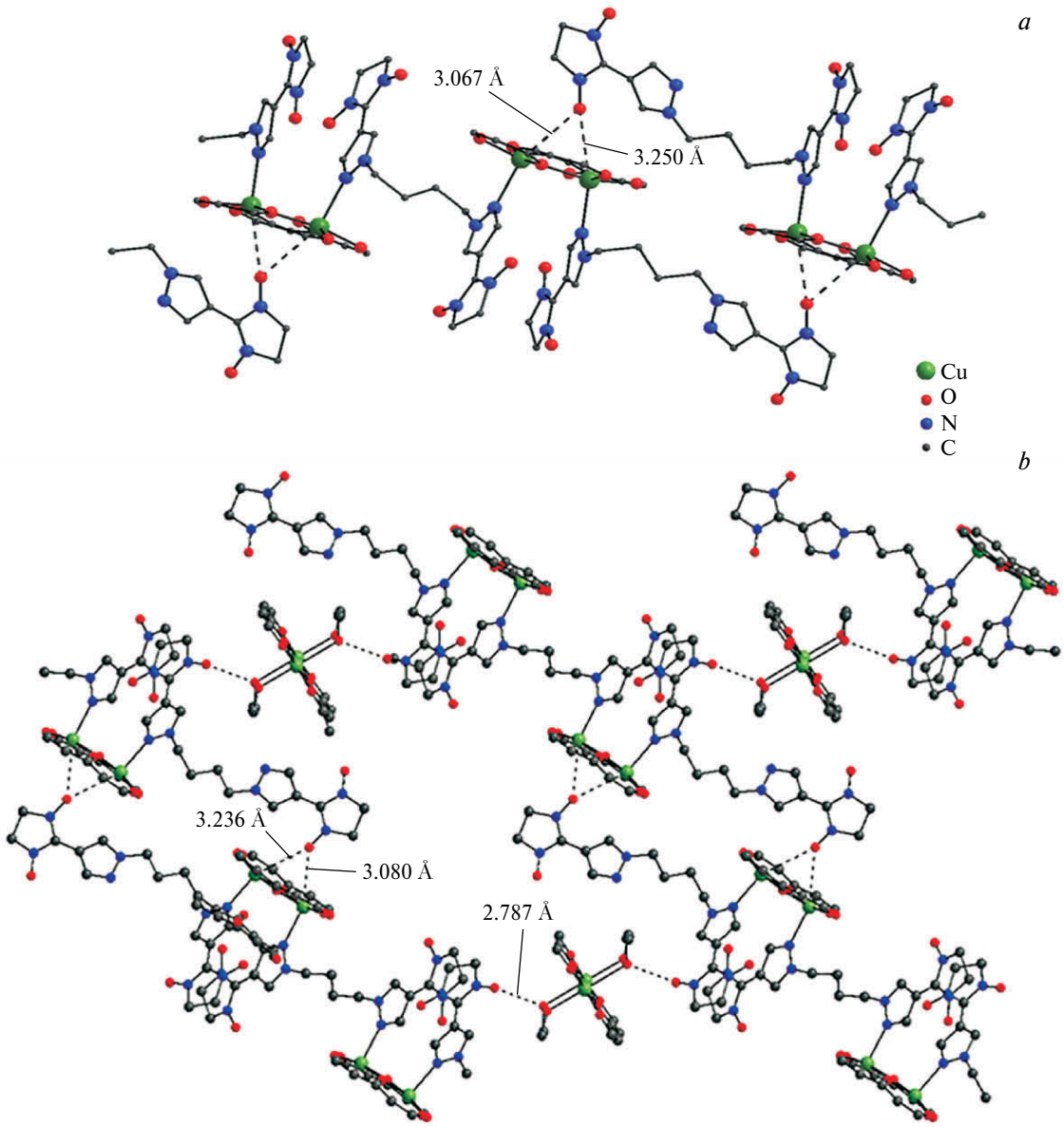

Fig. 3. Molecular structure of $[(Cu_2L_2)_2(NIT—Pz—(CH_2)_4—Pz—NIT)_3]$ (**4**) (*a*) and a fragment of the chain $\{[(Cu_2L_2)_2(NIT—Pz—(CH_2)_4—Pz—NIT)_3][Cu_2L_2(EtOH)_4]\}\cdot C_7H_8$ (**5**$\cdot C_7H_8$) (*b*).

short Cu...O_{NO} contacts in both structures, resulting in the square-bipyramidal coordination of the Cu atom (see Fig. 3, *b*).

In $[Cu_2L_2(NIT—p\text{-}NCC_6H_4)]$ (**6**), the coordination environment of the Cu atoms can be described as a square pyramid due to the coordination by bridging paramagnetic ligands located on opposite sides of the matrix (Fig. 4, *a*). As a result, head-to-tail zigzag chains (Cu—N, 2.299(4) Å; Cu—O, 2.481(3) Å) are formed. The crystallization from ethanol affords $[Cu_2L_2(NIT—p\text{-}NCC_6H_4)_2(EtOH)_2]$ (**7**), in which the O atoms of the ethanol molecules are involved in the coordination of the metal atoms, resulting in the octahedral environment (Cu—O_S, 2.361(2) and 2.341(2) Å). The ethanol molecules are involved in hydrogen bonding with the nitrile groups of NIT—*p*-NCC_6H_4 of adjacent complex molecules (see Fig. 4, *b*).

Unlike the reaction of $[Cu_2L_2]$ with NIT—*p*-NCC_6H_4, the reaction of $[Cu_2L_2]$ with the *meta*-derivative NIT—*m*-NCC_6H_4 in a ratio of either 1 : 1 or 1 : 2 in an Et_2O—hexane mixture affords the mononuclear complex $[Cu_2L_2(NIT—m\text{-}NCC_6H_4)_2]$ (**8**) (Fig. 5). In complex **8**, the nitroxides are coordinated through the O atom of the >N—O group ($d_{Cu—O}$ 2.393(4) Å).

The complex of $[Cu_2L_2]$ with NIT—*m*-NCC_6H_4 with the stoichiometry of 1 : 1 was obtained by crystallization from EtOH. In this case, the dinuclear matrix coordinates

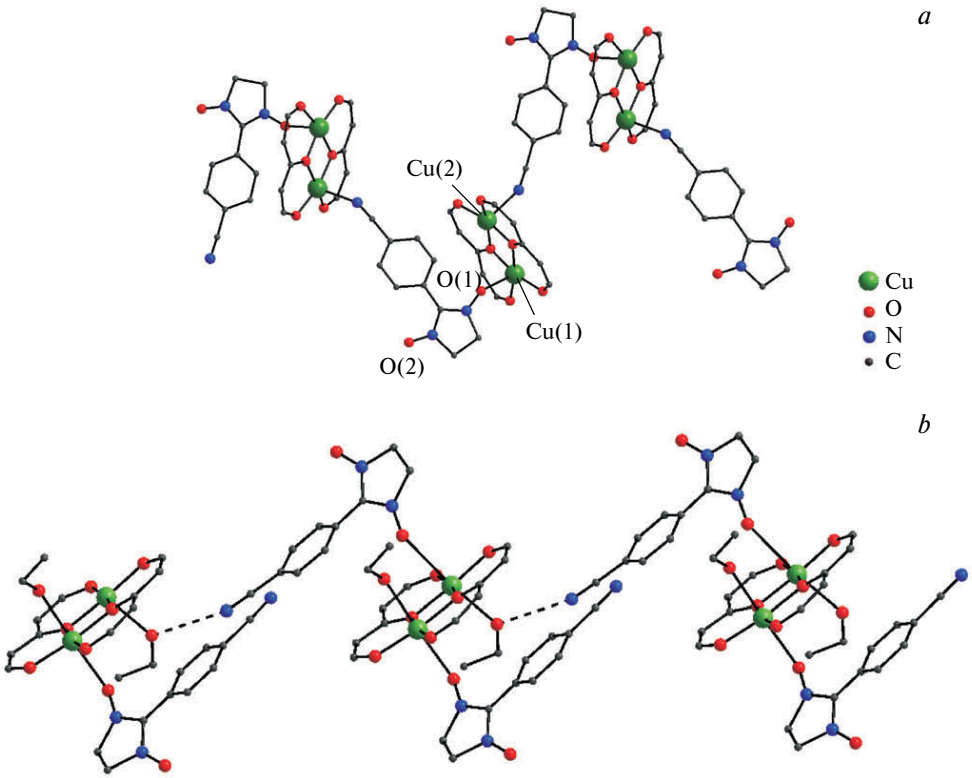

Fig. 4. Zigzag chains in $[Cu_2L_2(NIT—p\text{-}NCC_6H_4)]$ (**6**) (*a*) and $[Cu_2L_2(NIT—p\text{-}NCC_6H_4)_2(EtOH)_2]$ (**7**) (*b*).

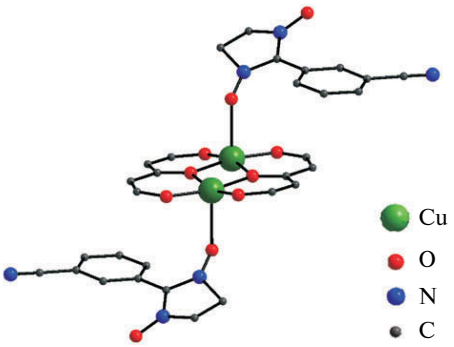

Fig. 5. Molecular structure of $[Cu_2L_2(NIT—m\text{-}NCC_6H_4)_2]$ (**8**).

two EtOH molecules, and the paramagnetic bridging NIT—*m*-NCC_6H_4 ligand links the $[Cu_2L_2(EtOH)_2]$ moieties together *via* hydrogen bonds between the OH groups of the coordinated ethanol molecules and the NO groups of the nitroxide to form chains (Fig. 6).

In the case of the nitroxide NIT—Me, which does not contain additional functional groups except nitronyl nitroxide, the complexes with the stoichiometry of both 1 : 1 and 1 : 2 were isolated. The molecular structure of complex **8** is similar to that of $[Cu_2L_2(NIT—Me)_2]$ (**10**) (Fig. 5). The complex with the ratio of 1 : 1 has a chain structure due to the bridging function of the paramagnetic ligand (Fig. 7).

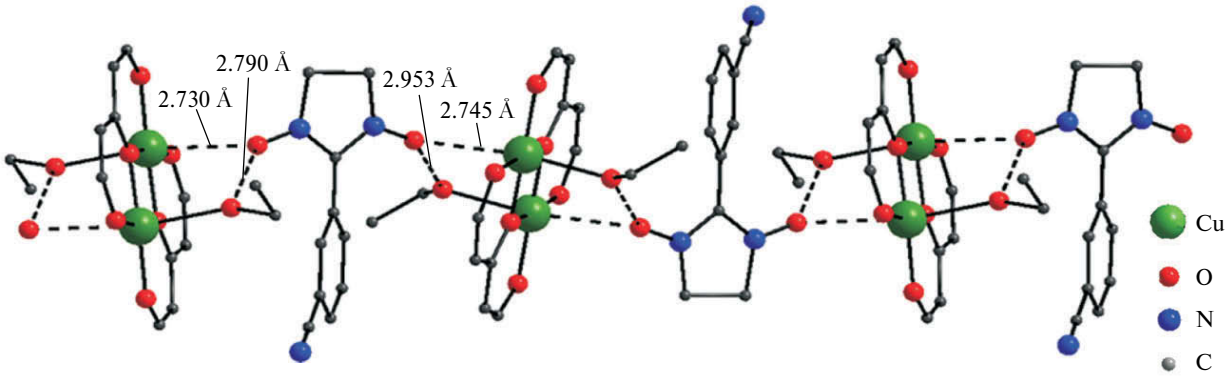

Fig. 6. Chain in the structure of $[Cu_2L_2(EtOH)_2(NIT—m\text{-}NCC_6H_4)]$ (**9**).

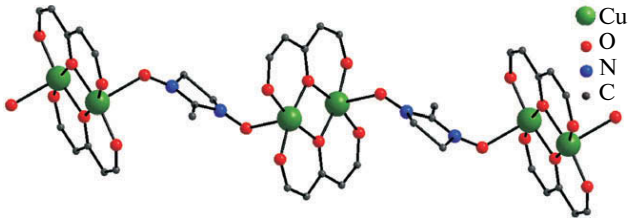

Fig. 7. Structure of the chain in $[Cu_2L_2(NIT—Me)]$ (**11**).

The main difference between the heterospin complexes of $[Mn_2L_2]$ with NIT—R and the above-described Cu^{II} compounds is that the central atoms in the former complexes are always in an octahedral environment. As a result, the complexes with the ratio $[Mn_2L_2]$: NIT—R = = 1 : 4 have a molecular structure, whereas the complexes with the ratio $[Mn_2L_2]$: NIT—R = 1 : 2 have a layer-polymeric structure. Figure 8 shows the molecular structures of $[Mn_2L_2(NIT—H)_4]$ (**12**) and $[Mn_2L_2(NIT—Me)_4]\cdot$ $\cdot$EtOH (**13**$\cdot$EtOH) in the crystals and a fragment of the

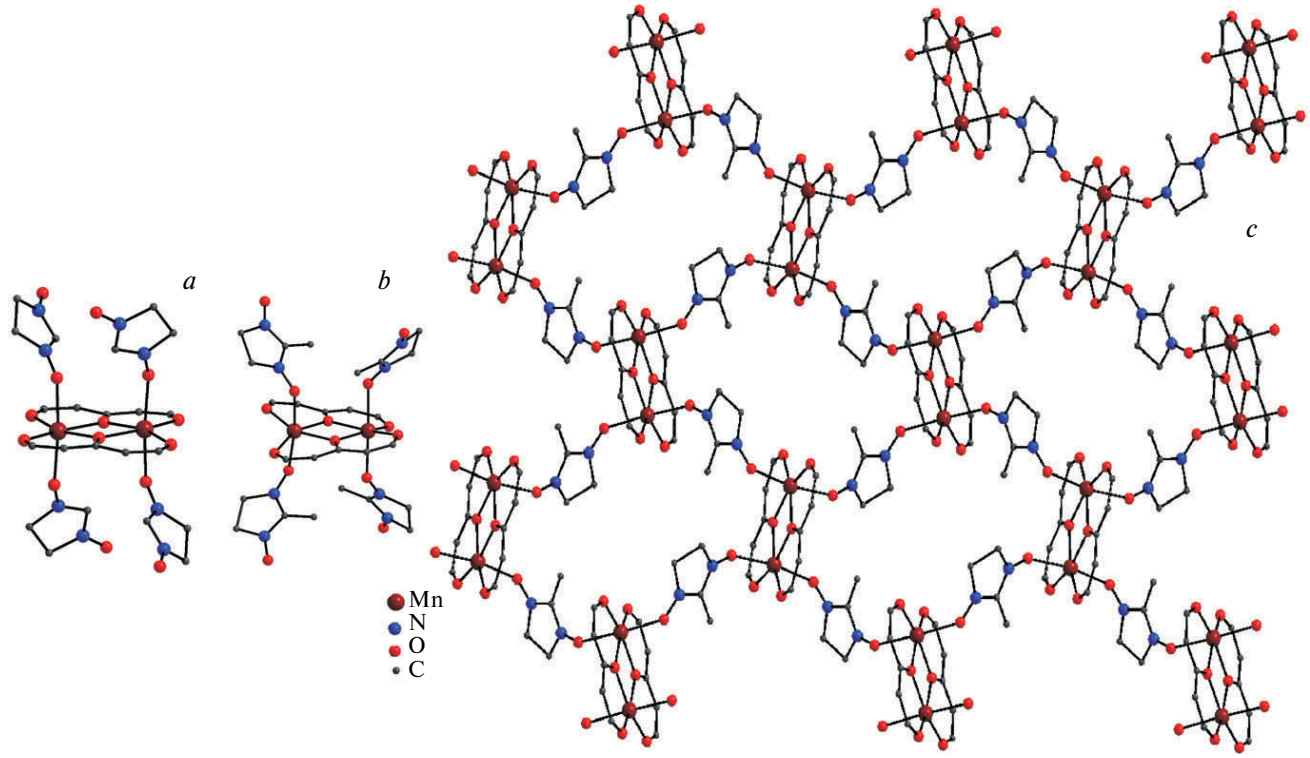

Fig. 8. Molecular structures of $[Mn_2L_2(NIT—H)_4]$ (**12**) (*a*) and $[Mn_2L_2(NIT—Me)_4]\cdot$(**13**) (*b*) and a fragment of the layer in $[Mn_2L_2(NIT—Me)_2]$ (**14**) (*c*).

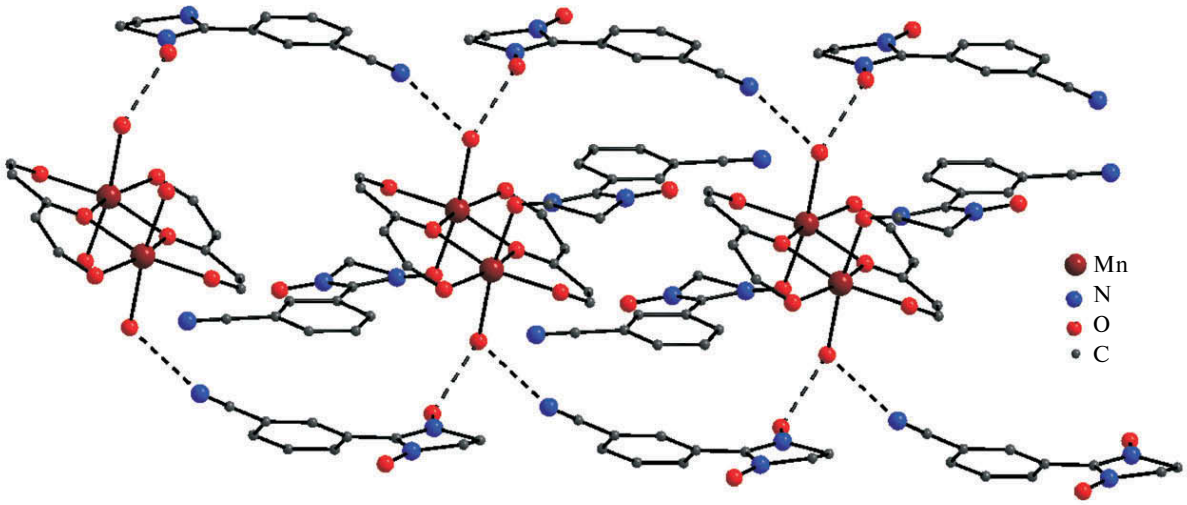

Fig. 9. Fragment of the ribbon in $\{[Mn_2L_2(H_2O)_2(NIT—m\text{-}NCC_6H_4)_2]\cdot 2(NIT—m\text{-}NCC_6H_4)\}$ (**16**).

Table 1. The M—O and M—N bond lengths (*d*) and the MON bond angles (ω) in the coordination units and the N—O bond lengths

Complex	*d*/Å					Angle MON/deg
	$M—O_{bridg}$	$M—O_{term}$	$M—O_{NIT}$	M—N	N—O	
1	1.922(2), 1.926(2)	1.874(2), 1.878(2)	—	—	—	—
2	1.966(4), 1.969(4)	1.906(4), 1.911(4)	—	2.269(5)	1.282(5), 1.281(6)	—
2 · Me_2CO · C_7H_8	1.969(3), 1.971(2)	1.902(3), 1.915(3)	—	2.251(3)	1.275(4), 1.274(4)	—
3 · CH_2Cl_2	1.940(3), 1.968(4)	1.903(4), 1.909(4)	—	2.218(5)	1.274(6), 1.263(6)	—
4 · $3C_7H_8$	1.931(6)—1.942(6)	1.866(6)—1.894(6)	3.067(9), 3.250(9)	2.272(9), 2.257(9)	1.23(1)—1.28(1)	—
5 · C_7H_8	1.935(5)—1.991(6)	1.887(5)—1.930(5)	3.236(6), 3.080(6)	2.288(5), 2.296(5)	1.278(8)—1.293(8)	—
6	1.942(3), 1.944(3), 1.944(3), 1.942(3)	1.891(3), 1.901(3), 1.892(3), 1.902(3)	2.482(3), 2.905(4)	2.300(4)	1.271(4), 1.281(4)	146.5(3), 119.2(3)
7	1.958(1), 1.962(1), 1.955(1), 1.970(1), 2.361(2)[a], 2.341(2)	1.909(1), 1.925(1), 1.912(1), 1.927(1)	2.443(2), 2.776(2)	—	1.294(2), 1.271(2), 1.283(2), 1.274(2)	135.3(1), 126.7(1)
8	1.946(3), 1.963(3)	1.906(3), 1.921(3)	2.392(4)	—	1.296(5), 1.274(6)	125.6(3)
9	1.943(3), 1.946(2), 1.939(2), 1.946(2), 2.326(3)[a], 2.282(3)	1.895(3), 1.897(3), 1.905(2), 1.905(2)	2.730(2), 2.745(2)	—	1.281(4), 1.277(4)	—
10	1.943(3), 1.949(3)	1.901(3), 1.905(3)	2.235(3)	—	1.274(5), 1.260(5)	137.4(3)
11	1.952(2), 1.957(2)	1.901(2), 1.913(2)	2.276(3)	—	1.287(4)	131.2(2)
12	2.186(4), 2.187(4)	2.068(5), 2.084(5)	2.142(5), 2.194(5)	—	1.288(7), 1.299(7), 1.312(7), 1.265(7)	137.8(5), 128.7(5)
13 · EtOH	2.192(2), 2.180(2)	2.089(3), 2.071(3)	2.166(3), 2.172(2)	—	1.301(3), 1.268(4), 1.299(4), 1.276(4)	127.6(2), 130.8(2)
14[b]	2.169(2), 2.185(2), 2.163(2), 2.180(2)	2.061(2), 2.074(2), 2.068(2), 2.074(2)	2.196(2), 2.198(2), 2.175(2), 2.200(2)	—	1.292(3), 1.288(3), 1.303(3), 1.287(3)	127.0(2), 137.0(2), 132.4(2), 142.1(2)
14a[c]	2.183(2), 2.189(2), 2.169(2), 2.189(2)	2.069(2), 2.078(2), 2.078(2), 2.082(2)	2.217(2), 2.221(2), 2.210(2), 2.230(2)	—	1.298(3), 1.288(3), 1.303(3), 1.289(3)	127.3(2), 139.5(2), 132.7(2), 144.3(2)
15	2.179(2), 2.184(2)	2.061(2), 2.080(2)	2.218(2), 2.252(3)	—	1.300(3), 1.288(3)	132.8(2), 144.9(2)
16	2.168(2), 2.171(2), 2.242(2)[d]	2.075(2), 2.077(2)	2.200(2)	—	1.293(3), 1.271(3), 1.285(3), 1.271(3)	123.9(2)

[a] $Cu—O_{EtOH}$.
[b] The experimental data at 200 K.
[c] The experimental data at 295 K.
[d] $Mn—O_{H_2O}$.

layer in isostructural $[Mn_2L_2(NIT\text{-}Me)_2]$ and $[Mn_2L_2(NIT\text{-}Et)_2]$. The layered structures $[Mn_2L_2(NIT{-}R)_2]$ (R = Me, Et) are formed due to the bridging function of nitroxide (Fig. 8, *c*). The matrices in these structures are almost planar (the maximum deviation of the atoms of the chelate rings is 0.09 Å). The $Mn{-}O_{NO}$ distances in the layer-polymeric complexes are somewhat longer (2.210(2)—2.232(2) Å) than those in the molecular complexes.

The complex $\{[Mn_2L_2(H_2O)_2(NIT{-}m\text{-}NCC_6H_4)_2]\cdot 2(NIT{-}m\text{-}NCC_6H_4)\}$ (**16**) (Fig. 9), which was obtained with the use of the starting ratio $[Mn_2L_2]$: NIT—*m*-NCC_6H_4 of 1 : 1 or 1 : 2 and, finally, the ratio of 1 : 4 optimal for the stoichiometry of this phase, has a specific structure in the solid state. The coordination environment of the Mn atom can be described as a distorted octahedron whose axial positions are occupied by the O atom of one NO group and the H_2O molecule hydrogen-bonded to the N_{CN} and O_{NO} atoms of the outer-sphere NIT—*m*-NCC_6H_4 ligand. As a result, the solid phase of the heterospin complex is built of infinite ribbons with nitroxide molecules at the edges.

In all the complexes under consideration, the distances between the paramagnetic centers of adjacent molecules or adjacent chains (layers) are large. In the Mn complexes, these distances are larger than 4.5 Å; the shortest distances ($Cu...O_{NO}$) are observed in the structure of **9** (2.730(3) and 2.745(3) Å). Consequently, main exchange interactions between unpaired electrons should exist inside heterospin molecules or heterospin chains (layers).

The investigation of the magnetic properties of $Cu_2L_2\cdot 2C_7H_8$ showed that in the solid phase there is a strong antiferromagnetic exchange coupling between the unpaired electrons of the Cu^{II} ions inside the dinuclear matrix (Fig. 10). This coupling causes a rapid decrease in μ_{eff} with a decrease in the temperature. Based on the estimation of the exchange coupling parameters with the use of the exchange-coupled pair model $\chi = 2Ng^2\beta^2/(kT[3+\exp(-2J/kT)])$,[20] the optimum *g* factor and J/k are 2.08 and −385 K, respectively. It should be noted that there are indirect exchange interactions in the dinuclear matrices through the Cu—O—Cu channels with the involvement of the bridging O atom (the direct exchange between the unpaired electrons of paramagnetic centers occurs only if the O atoms of nitroxide groups are coordinated to Cu^{II} or Mn^{II} ions).

For complex **11**, the magnetic moment μ_{eff} gradually decreases with a decrease in the temperature from 2.08 μ_B at 300 K to 1.77 μ_B at 200 K, after which it remains virtually unchanged down to 15 K (see Fig. 10). The magnetic moment μ_{eff} on the plateau is 1.77 μ_B and it is in good agreement with the theoretical value (1.73 μ_B) for one paramagnetic center with the spin $S = 1/2$ and $g = 2$, which corresponds to the spin of the nitroxide. A decrease in μ_{eff} in the initial region is indicative of the strong antiferromagnetic

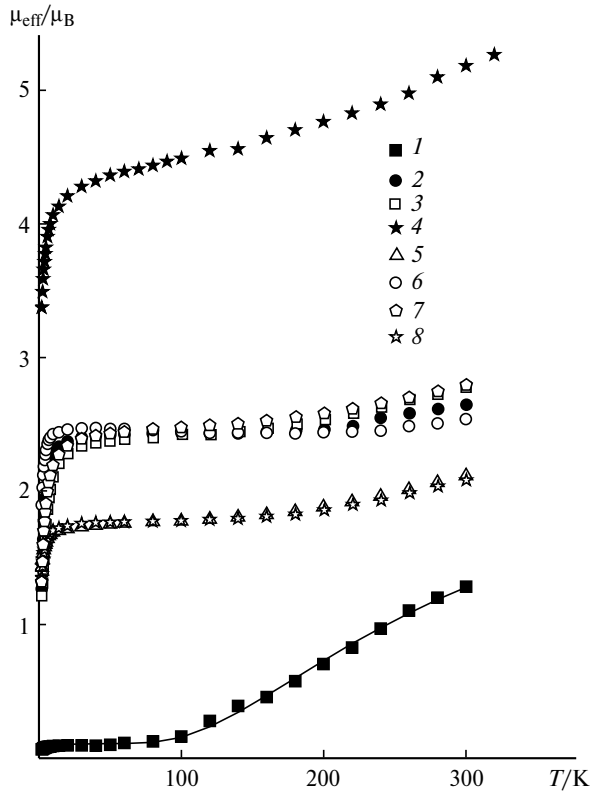

Fig. 10. Temperature dependences of the effective magnetic moment (μ_{eff}) for the Cu^{II} complexes: **1** (*1*), **2**·C_7H_8·Me_2CO (*2*), **3**·CH_2Cl_2 (*3*), **4**·$3C_7H_8$ (*4*), **6** (*5*), **8** (*6*), **10** (*7*), and **11** (*8*). The points correspond to the experimental data, and the calculated data are indicated by the solid line.

exchange coupling between the unpaired electrons of the Cu^{II} ions; the exchange parameter can be estimated as $|J/k| > 500$ K, which is substantially larger than that in the starting dinuclear matrix. The magnetic properties of complexes **6** and **11** are virtually identical (see Fig. 10).

Complexes **2**·Me_2CO·C_7H_8, **3**·CH_2Cl_2, **10**, and **8** are characterized by similar plots $\mu_{eff}(T)$ (see Fig. 10). The magnetic moment μ_{eff} gradually decreases with a decrease in the temperature and reaches a plateau $\mu_{eff} = 2.46$ μ_B at ~200 K, which is in good agreement with the theoretical spin-only value (2.45 μ_B) for two non-interacting spins $S = 1/2$ with $g = 2$. Therefore, the unpaired electrons of the nitroxide centers make the major contribution to the magnetic susceptibility of the solid phases under consideration. The antiferromagnetic exchange coupling between the unpaired electrons of the Cu^{II} ions in these complexes is large ($|J/k| > 500$ K).

The temperature dependence of μ_{eff} for complex **4** with the diradical has the same character (see Fig. 10) as that observed for the other complexes based on the matrix $[Cu_2L_2]$. The magnetic moment μ_{eff} gradually decreases with a decrease in the temperature and approaches $\mu_{eff} \approx 4.4$ μ_B. This value is in good agreement with the

theoretical spin-only value of 4.24 μ_B (at $g = 2$), which was obtained by the summation of the contributions of six noninteracting electrons of three diradicals.

Therefore, the strong antiferromagnetic coupling between the unpaired electrons of the Cu^{II} ions in $[Cu_2L_2]$ is not only retained but is even increased upon the coordination of nitroxides. As a result, the spins of the Cu^{II} ions in the matrices are almost completely paired, and only the unpaired electrons of NIT—R make the major contribution to the magnetic susceptibility.

In $[Mn_2L_2]$, the antiferromagnetic coupling predominates at temperatures below 100 K (Fig. 11). The calculations in terms of the dimer model for paramagnetic centers with the spin 5/2 confirmed this fact. The exchange coupling parameter (J/k) and the g factor are −1.86 K and 1.96, respectively.

For complex **12**, the magnetic moment μ_{eff} gradually decreases with a decrease in the temperature, reaches a small plateau of ~5.54 μ_B at 100 K, and then again decreases (Fig. 11). This character of the plot $\mu_{eff}(T)$ can be interpreted by assuming a strong antiferromagnetic exchange coupling between the unpaired electrons of the Mn^{II} ions and the coordinated nitroxide groups. In this case, the value of 5.54 μ_B is in good agreement with the theoretical value of 5.48 μ_B, which corresponds to the paramagnetic system consisting of two weakly interacting paramagnetic centers with spins $S = 3/2$. In molecules **12**, these centers appear due to the compensation of the spins of two unpaired electrons of each high-spin Mn^{II} ion by the spins of two coordinated NIT—H ligands.

For complexes **14** and **15**, the temperature dependences of μ_{eff} are virtually identical. The magnetic moments μ_{eff} gradually increase from 8.39 and 8.53 μ_B, respectively (300 K), with a decrease in the temperature, reach a maximum of 11.12 μ_B (80 K) and 11.12 μ_B (100 K), and then decrease (see Fig. 11). An increase in μ_{eff} in the initial step indicates that the ferromagnetic exchange between the unpaired electrons of NIT—R and Mn^{II} ions predominate. A decrease in μ_{eff} after the achievement of the maximum can be attributed to the antiferromagnetic exchange coupling in the dinuclear matrix.

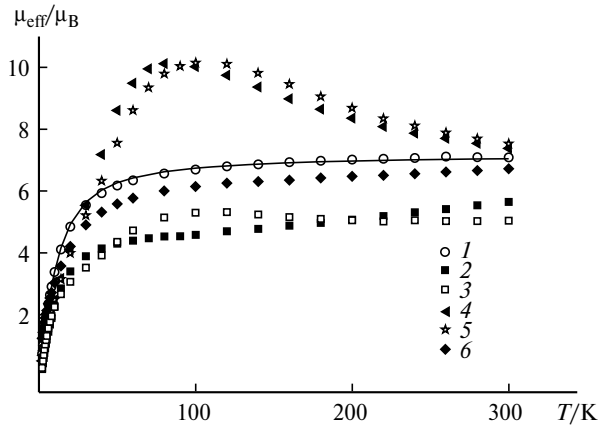

Fig. 11. Temperature dependences of the effective magnetic moment μ_{eff} for the Mn^{II} complexes: $[Mn_2L_2] \cdot 4H_2O$ (*1*), **12** (*2*), **13** (*3*), **14** (*4*), **15** (*5*), and **16** (*6*). The points correspond to the experimental data, and the calculated data are indicated by the solid line.

For complex **16**, the dependence $\mu_{eff}(T)$ is in good agreement with the structural data. The magnetic moment μ_{eff} slowly decreases with a decrease in the temperature from 7.72 μ_B at 300 K to 7.01 μ_B at 80 K and then strongly decreases (see Fig. 11). In the temperature range of 200—100 K, the magnetic moments μ_{eff} are close to 7.39 μ_B, which corresponds to the contribution of four weakly interacting centers to the magnetic susceptibility; two of these centers have $S = 4/2$ and the other two centers have $S = 1/2$ (at $g = 2$). This indicates that there is the strong antiferromagnetic exchange coupling between the spins of Mn^{II} and coordinated nitroxides in complex **16**. The antiferromagnetic couping between the spins of the hydrogen-bonded Mn^{II} ions and NIT—*m*-CNC_6H_4 is substantially weaker and is observed at temperatures below 100 K.

The results of magnetic measurements for the dinuclear Mn^{II} complexes with nitroxides lead to the conclusion that the strongest exchange coupling exists between the unpaired electrons of the metal ions and the coordinated NIT—R ligands. It is important that not only antiferromagnetic exchange but also ferromagnetic exchange coupling (as in complexes **14** and **15**) can exist.

Therefore, we synthesized and structurally characterized dinuclear heterospin Cu^{II} and Mn^{II} 1,1,1,7,7,7-hexafluoroheptane-2,4,6-trionate complexes with nitroxides. Heterospin complexes of both $[Cu_2L_2]$ and $[Mn_2L_2]$ with the direct coordination of nitroxide groups were isolated, *i.e.*, heterospin magnetic clusters with high-energy exchange interactions were synthesized. Consequently, these compounds are promising in the molecular design of magnets. The following magnetochemical features of the compounds should be taken into account. In the $[Cu_2L_2]$ molecules, the antiferromagnetic exchange coupling predominates in the temperature range of 2—300 K, whereas this type of coupling in the $[Mn_2L_2]$ matrix becomes significant only at temperatures below 100 K. The magnetic properties of the heterospin complexes of $[Cu_2L_2]$ with NIT—R are also determined by the intramatrix antiferromagnetic exchange; in the complexes of $[Mn_2L_2]$ with NIT—R, the coordination mode of nitroxides is a decisive factor.

Experimental

1,1,1,7,7,7-Hexafluoroheptane-2,4,6-trione monohydrate was synthesized by the modified Claisen condensation.[21]

Synthesis of dinuclear matrices $[M_2L_2]$

Bis(μ_2-1,1,1,7,7,7-hexafluoroheptane-2,4,6-trionato)dicopper(II) monohydrate, $[Cu_2L_2] \cdot H_2O$. A solution of 1,3,5-triketone

monohydrate (8.04 g, 30 mmol) in water (30 mL) was added to a solution of $Cu_2(CH_3COO)_4 \cdot 2H_2O$ (10 g, 25 mmol) in water (100 mL). The reaction mixture was stirred for 2 h and kept for 16 h. The precipitate was filtered off, repeatedly washed with water, dried on the filter, washed with boiling chloroform (3×20 mL), and twice sublimed. The dark-green crystals that formed were dried in air to a constant weight. The yield was 7.02 g (73%). Found (%): C, 26.1; H 1.1; F, 35.4. $C_{14}H_6O_7F_{12}Cu_2$. Calculated (%): C, 26.2; H, 0.9; F, 35.6.

Bis(μ_2-1,1,1,7,7,7-hexafluoroheptane-2,4,6-trionato)dimanganese(II) tetrahydrate, $[Mn_2L_2] \cdot 4H_2O$. A solution of 1,3,5-triketone hydrate (5.36 g, 20 mmol) and $CH_3COONa \cdot 3H_2O$ (5.50 g, 40.4 mmol) in water (30 mL) was slowly added with vigorous stirring to a solution of $MnCl_2 \cdot 4H_2O$ (5.94 g, 30 mmol) in water (30 mL). The reaction mixture was stirred for 4 h and kept for 16 h. The precipitate was filtered off, repeatedly washed with water, dried on the filter, washed with boiling chloroform (3×20 mL), and twice reprecipitated from methanol. The cream-colored powder was dissolved in diethyl ether (10 mL). Then toluene (20 mL) was added, and diethyl ether was slowly evaporated at room temperature. The crystals that formed were filtered off, repeatedly recrystallized, dried *in vacuo*, and then dried in air to a constant weight for two days. The yield was 3.78 g (56%). Found (%): C, 24.6; H, 1,7; F, 33.6. $C_{14}H_{10}O_{10}F_{12}Mn_2$. Calculated (%): C, 24.9; H, 1.5; F, 33.7.

Synthesis of heterospin complexes

***catena*-{(μ_2-2,4,4,5,5-Pentamethyl-4,5-dihydro-1*H*-imidazole-3-oxide-1-oxyl)bis(μ_2-1,1,1,7,7,7-hexafluoroheptane-2,4,6-trionato)dicopper(II)}, $[Cu_2L_2(NIT—Me)]$ (11).** A mixture of $[Cu_2L_2] \cdot H_2O$ (0.0500 g, 0.08 mmol) and NIT—Me (0.0134 g, 0.08 mmol) was dissolved in diethyl ether (2 mL) and filtered. Then toluene (3 mL) was added, and the reaction mixture was kept in an open flask in a refrigerator overnight. The dark-red crystals that formed were filtered off, washed with cold toluene, and dried in air. The yield was 42%. Found (%): C, 33.3; H, 2.0; N, 3.7; F, 28.2. $C_{22}H_{19}N_2O_8F_{12}Cu_2$. Calculated (%): C, 33.3; H, 2.4; N, 3.5; F, 28.7.

Bis[2,4,4,5,5-pentamethyl-4,5-dihydro-1*H*-imidazole-3-oxide-1-oxyl]bis(μ_2-1,1,1,7,7,7-hexafluoroheptane-2,4,6-trionato)dicopper(II), $[Cu_2L_2(NIT—Me)_2]$ (10). A mixture of $[Cu_2L_2] \cdot H_2O$ (0.0500 g, 0.08 mmol) and NIT—Me (0.0267 g, 0.16 mmol) was dissolved in diethyl ether (5 mL) and filtered. Then hexane (3 mL) was added, and the reaction mixture was kept in an open flask in a refrigerator overnight. The dark-red crystalline intergrowths that formed were filtered off, washed with cold hexane, and dried in air. The yield was 56%. Found (%): C, 37.2; H, 3.8; N, 6.1; F, 23.6. $C_{30}H_{34}N_4O_{10}F_{12}Cu_2$. Calculated (%): C, 37.3; H, 3.6; N, 5.8; F, 23.6.

Bis[1-methyl-4-(4,4,5,5-tetramethyl-3-oxide-1-oxyl-4,5-dihydro-1*H*-imidazol-2-yl)-1*H*-pyrazole]bis(μ_2-1,1,1,7,7,7-hexafluoroheptane-2,4,6-trionato)dicopper(II) acetone toluene solvate, $[Cu_2L_2(NIT—PzMe)_2] \cdot Me_2CO \cdot C_7H_8$ (2 · $Me_2CO \cdot C_7H_8$). A mixture of $[Cu_2L_2] \cdot H_2O$ (0.0500 g, 0.08 mmol) and NIT—PzMe (0.0370 g, 0.16 mmol) was dissolved in acetone (2 mL). Then toluene (5 mL) was slowly added, and the reaction mixture was kept in an open flask for one day. The black octahedral crystals that formed were filtered off, washed with cold toluene, and dried in air. The yield was 62%. Calculated for the desolvated compound (%): C, 39.4; H, 3.5; N, 10.2; F, 20.8. Found (%): C, 39.8; H, 3.8; N, 10.1; F, 20.2. $C_{36}H_{38}N_8O_{10}F_{12}Cu_2$. The synthesis in an acetone—hexane mixture afforded **$[Cu_2L_2(NIT\text{-}PzMe)_2]$ (2)** as the solid product in ~90% yield.

{μ_2-1,4-Bis[4-(4,4,5,5-tetramethyl-3-oxide-1-oxyl-4,5-dihydro-1*H*-imidazol-2-yl)pyrazol-1-yl]butane-*N*,*N*′}bis{1,4-bis[4-(4,4,5,5-tetramethyl-3-oxide-1-oxyl-4,5-dihydro-1*H*-imidazol-2-yl)pyrazol-1-yl]butane-*N*}bis[bis(μ_2-1,1,1,7,7,7-hexafluoroheptane-2,4,6-trionato)dicopper(II)] tritoluene solvate, $[(Cu_2L_2)_2(NIT—Pz—(CH_2)_4—Pz—NIT)_3] \cdot 3C_7H_8$ (4 · $3C_7H_8$). A mixture of $[Cu_2L_2] \cdot H_2O$ (0.0500 g, 0.08 mmol) and NIT—Pz—$(CH_2)_4$—Pz—NIT (0.0585 g, 0.12 mmol) was dissolved in acetone (2 mL). Then toluene (4 mL) was added, and the reaction mixture was kept in an open flask in a refrigerator for 2 days. The dark-blue crystals that formed were filtered off, washed with cold toluene, and dried in air for 1 min. The yield was 30%. Found (%): C, 44.1; H, 4.6; N, 12.6; F, 16.6. $C_{100}H_{116}N_{24}O_{24}F_{24}Cu_4$. Calculated for the desolvated compound (%): C, 43.7; H, 4.3; N, 12.2; F, 16.6.

The recrystallization of the complex from ethanol afforded **{μ_2-1,4-bis[4-(4,4,5,5-tetramethyl-3-oxide-1-oxyl-4,5-dihydro-1*H*-imidazol-2-yl)pyrazol-1-yl]butane-*N*,*N*′}bis{1,4-bis[4-(4,4,5,5-tetramethyl-3-oxide-1-oxyl-4,5-dihydro-1*H*-imidazol-2-yl)pyrazol-1-yl]butane-*N*}bis[bis(μ_2-1,1,1,7,7,7-hexafluoroheptane-2,4,6-trionato)dicopper(II)]bis(μ_2-1,1,1,7,7,7-hexafluoroheptane-2,4,6-trionato)tetraethanoldicopper(II) toluene solvate, $\{[(Cu_2L_2)_2(NIT—Pz—(CH_2)_4—Pz—NIT)_3][Cu_2L_2(EtOH)_4]\} \cdot \cdot C_7H_8$ (5 · C_7H_8).**

Bis[3-(4,4,5,5-tetramethyl-3-oxide 1-oxyl-4,5-dihydro-1*H*-imidazole-2-yl)-pyridine]bis(μ_2-1,1,1,7,7,7-hexafluoroheptane-2,4,6-trionato)dicopper(II) dichloromethane solvate, $[Cu_2L_2(NIT—m\text{-}C_5H_4N)_2] \cdot CH_2Cl_2$ (3 · CH_2Cl_2). A mixture $[Cu_2L_2] \cdot H_2O$ (0.0500 g, 0.08 mmol) and NIT—*m*-C_5H_4N (0.0365 g, 0.16 mmol) was dissolved in CH_2Cl_2 (2 mL). Then heptane (2 mL) was added, and the reaction mixture was kept in an open flask for 7 h. Large dark-blue crystals that formed were filtered off, washed with a cold CH_2Cl_2—heptane mixture (1 : 1), and dried in air for 1 min. The yield was 71%. Found (%): C, 41.3; H, 3.3; N, 7.8; F, 20.3. $C_{38}H_{36}N_6O_{10}F_{12}Cu_2$. Calculated for the desolvated compound (%): C, 41.8; H, 3.3; N, 7.7; F, 20.9.

***catena*-{μ_2-2-(4-Cyanophenyl)-4,4,5,5-tetramethyl-4,5-dihydro-1*H*-imidazole-3-oxide-1-oxyl-*N*,*O*)bis(μ_2-1,1,1,7,7,7-hexafluoroheptane-2,4,6-trionato)dicopper(II)}, $[Cu_2L_2(NIT—p\text{-}NCC_6H_4)]$ (6).** A mixture $[Cu_2L_2] \cdot H_2O$ (0.0500 g, 0.08 mmol) and NIT—*p*-NCC_6H_4 (0.0183 g, 0.08 mmol) was dissolved in diethyl ether (5 mL) and filtered. Then hexane (3 mL) was added, and the reaction mixture was kept in an open flask in a refrigerator overnight. The crystalline dark-blue intergrowths that formed were filtered off, washed with cold hexane, and dried in air. The yield was 60%. Found (%): C, 38.5; H, 2.6; N, 5.1; F, 25.3. $C_{28}H_{20}N_3O_8F_{12}Cu_2$. Calculated (%): C, 38.2; H, 2.3; N, 4.8; F, 25.9. The recrystallization of the complex from ethanol afforded **bis[2-(4-cyanophenyl)-4,4,5,5-tetramethyl-4,5-dihydro-1*H*-imidazole-3-oxide-1-oxyl-*O*]bis(μ_2-1,1,1,7,7,7-hexafluoroheptane-2,4,6-trionato)diethanoldicopper(II), $[Cu_2L_2(NIT—p\text{-}NCC_6H_4)_2(EtOH)_2]$ (7).**

Bis[2-(3-cyanophenyl)-4,4,5,5-tetramethyl-4,5-dihydro-1*H*-imidazole-3-oxide-1-oxyl-*O*]bis(μ_2-1,1,1,7,7,7-hexafluoroheptane-2,4,6-trionato)dicopper(II), $[Cu_2L_2(NIT—m\text{-}NCC_6H_4)_2]$ (8) was synthesized analogously. Dark-blue crystals formed. The yield was 50%. Found (%): C, 44.8; H, 2.6; N, 7.6; F, 20.2. $C_{42}H_{36}N_6O_{10}F_{12}Cu_2$. Calculated (%): C, 44.3; H, 3.2; N, 7.4; F, 20.0.

2-[(3-Cyanophenyl)-4,4,5,5-tetramethyl-4,5-dihydro-1*H*-imidazole-3-oxide-1-oxyl]bis(μ$_2$-1,1,1,7,7,7-hexafluoroheptane-2,4,6-trionato)diethanoldicopper(II), [Cu$_2$L$_2$(EtOH)$_2$]·NIT—*m*-NCC$_6$H$_4$ (9). A mixture of [Cu$_2$L$_2$]·H$_2$O (0.0500 g, 0.08 mmol) and NIT—*m*-NCC$_6$H$_4$ (0.0183 g, 0.08 mmol) was dissolved in ethanol (5 mL) and kept in an open flask for one day. The dark-blue crystals that formed were filtered off, washed with cold ethanol, and dried in air. The yield was 40%. Found (%): C, 38.4; H, 4.3; N, 4.6; F,24.6. $C_{30}H_{32}N_3O_{10}F_{12}Cu_2$. Calculated (%): C, 37.9; H, 3.4; N, 4.4; F, 24.0.

Tetrakis[4,4,5,5-pentamethyl-4,5-dihydro-1*H*-imidazole-3-oxide-1-oxyl]bis(μ$_2$-1,1,1,7,7,7-hexafluoroheptane-2,4,6-trionato)dimanganese(II), [Mn$_2$L$_2$(NIT—H)$_4$] (12). A solution of NIT—H (0.0464 g, 0.3 mmol) in diethyl ether (3 mL) was added to a solution of [Mn$_2$L$_2$]·4H$_2$O (0.0500 g, 0.07 mmol) in diethyl ether (2 mL). Dark-red crystals immediately formed. The crystals were filtered off, washed with cold diethyl ether, and dried in air. The yield was 53%. Found (%): C, 41.1; H, 4.7; N, 9.3; F, 19.0. $C_{42}H_{56}N_8O_{14}F_{12}Mn_2$. Calculated (%): C, 40.8; H, 4.6; N, 9.1; F, 18.5.

Tetrakis[2,4,4,5,5-pentamethyl-4,5-dihydro-1*H*-imidazole-3-oxide-1-oxyl]bis(μ$_2$-1,1,1,7,7,7-hexafluoroheptane-2,4,6-trionato)dimanganese(II), [Mn$_2$L$_2$(NIT—Me)$_4$] (13) was synthesized analogously. Dark-red fiber-like crystals were obtained. The yield was 61%. Found (%): C, 43.0; H, 5.4; N, 8.8; F, 18.1. $C_{46}H_{64}N_8O_{14}F_{12}Mn_2$. Calculated (%): C, 42.8; H, 5.0; N, 8.7; F, 17.7. Crystals of **[Mn$_2$L$_2$(NIT—Me)$_4$]·EtOH** suitable for X-ray diffraction were grown by recrystallization of the complex from ethanol.

***catena*-{Bis(μ$_2$-2,4,4,5,5-pentamethyl-4,5-dihydro-1*H*-imidazole-3-oxide-1-oxyl)bis(μ$_2$-1,1,1,7,7,7-hexafluoroheptane-2,4,6-trionato)dimanganese(II)}, [Mn$_2$L$_2$(NIT—Me)$_2$] (14).** A solution of NIT—Me (0.0252 g, 0.15 mmol) in diethyl ether (3 mL) was added to a solution of [Mn$_2$L$_2$]·4H$_2$O (0.0500 g, 0.07 mmol) in diethyl ether (2 mL). After 3 h, the dark-red crystals that formed were filtered off, washed with cold diethyl ether, and dried in air. The yield was 39%. Found (%): C, 38.8; H, 3.8; N, 6.0; F, 24.4. $C_{30}H_{34}N_4O_{10}F_{12}Mn_2$. Calculated (%): C, 38.0; H, 3.6; N, 5.9; F, 24.0.

***catena*-{Bis(μ$_2$-2-ethyl-4,4,5,5-tetramethyl-4,5-dihydro-1*H*-imidazole-3-oxide-1-oxyl)bis(μ$_2$-1,1,1,7,7,7-hexafluoroheptane-2,4,6-trionato)dimanganese(II)}, [Mn$_2$L$_2$(NIT—Et)$_2$] (15).** A mixture of [Mn$_2$L$_2$]·4H$_2$O (0.0500 g, 0.07 mmol) and NIT—Et (0.0273 g, 0.15 mmol) was dissolved in diethyl ether (3 mL) and filtered. Then hexane (2 mL) was added, and the reaction mixture was kept in an open flask in a refrigerator for 4 h. The dark-red crystals that formed were filtered off, washed with a cold diethyl ether—hexane mixture (1 : 1), and dried in air. The yield was 73%. Found (%): C, 39.5; H, 3.9; N, 5.8; F, 24.2. $C_{32}H_{38}N_4O_{10}F_{12}Mn_2$. Calculated (%): C, 39.4; H, 3.9; N, 5.7; F, 23.4.

Bis[2-(3-cyanophenyl)-4,4,5,5-tetramethyl-4,5-dihydro-1*H*-imidazole-3-oxide-1-oxyl]bis[2-(3-cyanophenyl)-4,4,5,5-tetramethyl-4,5-dihydro-1*H*-imidazole-3-oxide-1-oxyl-*O*]bis(μ$_2$-1,1,1,7,7,7-hexafluoroheptane-2,4,6-trionato)diaquadimanganese(II), [Mn$_2$L$_2$(NIT—*m*-NCC$_6$H$_4$)$_2$(H$_2$O)$_2$]·2NIT—*m*-NCC$_6$H$_4$ (16). A solution of NIT—*m*-NCC$_6$H$_4$ (0.0762 g, 0.30 mmol) in C$_6$H$_6$ (2 mL) was added to a solution of [Mn$_2$L$_2$]·4H$_2$O (0.0500 g, 0.07 mmol) in diethyl ether (2 mL). After 5 h, the crystals that formed were filtered off, washed with cold diethyl ether, and dried in air. The yield was 62%. Found (%): C, 50.5; H, 4.3; N, 10.2; F, 13.2. $C_{70}H_{72}N_{12}O_{16}F_{12}Mn_2$. Calculated (%): C, 50.2; H, 4.3; N, 10.0; F, 13.6.

Table 2. Crystallographic parameters and the X-ray diffraction data collection and refinement statistics for compounds **1**—**5**

Parameter	**1**	**2**	**2**·Me$_2$CO·C$_7$H$_8$	**3**·CH$_2$Cl$_2$	**4**·3C$_7$H$_8$	**5**·C$_7$H$_8$
Molecular weight	807.52	1097.82	1248.04	1176.74	1512.37	3647.98
T/K	293	298	298(2)	293	293	293
Space group	*C*2/*m*	*Pnna*	*Pnna*	$P\bar{1}$	$P\bar{1}$	$P\bar{1}$
a/Å	19.568(8)	12.657(1)	12.764(4)	8.910(3)	14.063(3)	14.375(3)
b/Å	18.917(8)	18.929(2)	18.449(5)	10.734(4)	14.544(3)	14.426(2)
c/Å	9.658(4)	22.604(3)	23.236(7)	13.062(5)	18.451(4)	20.251(4)
α/deg	—	—	—	76.294(6)	112.03(3)	80.443(5)
β/deg	115.661(6)	—	—	84.144(6)	94.15(3)	80.302(5)
γ/deg	—	—	—	76.863(6)	102.99(3)	76.583(8)
V/Å^3	3223(2)	5415.9(11)	5472(3)	1180.3(7)	3357(1)	3991.1(13)
Z	4	4	4	2	2	1
d_{calc}/g cm^{-3}	1.664	1.346	1.515	1.655	1.496	1.518
μ/mm^{-1}	1.428	0.879	0.881	1.122	0.735	0.904
θ-Scan range/deg	1.58—23.28	1.80—23.33	1.82—23.33	2.27—26.47	1.76—23.64	1.90—26.41
I_{hkl} measured/independent	11997/2375	39118/3912	40007/3967	8005/4800	25413/9784	27968/15554
R_{int}	0.0397	0.0913	0.0712	0.0731	0.0632	0.0504
Refined parameters	286	353	405	352	967	1047
GOOF	1.021	1.054	0.998	0.913	0.681	0.971
R_1	0.0365	0.0661	0.0483	0.0578	0.0646	0.0618
wR_2 based on reflections with $I > 2\sigma(I)$	0.0987	0.1887	0.1073	0.1603	0.1078	0.1308
R_1	0.0489	0.1024	0.0747	0.0861	0.3155	0.1414
wR_2 (based on all data)	0.1067	0.2056	0.1271	0.2251	0.1651	0.1628

Table 3. Crystallographic parameters and the X-ray diffraction data collection and refinement statistics for compounds **6—11**

Parameter	**6**	**7**	**8**	**9**	**10**	**11**
Molecular weight	881.55	1231.98	1139.84	723.69	965.69	794.47
T/K	298	150	293	293	293	298
Space group	$P2_1/n$	$P\bar{1}$	$P\bar{1}$	$P\bar{1}$	$P2_1/n$	$C2/c$
a/Å	11.4981(14)	9.9992(3)	8.1770(16)	10.406(2)	7.1353(17)	20.454(4)
b/Å	15.7557(19)	12.8045(3)	10.833(2)	11.555(2)	28.032(8)	8.1842(15)
c/Å	18.504(2)	21.8111(7)	14.442(3)	16.890(4)	10.192(3)	18.934(3)
α/deg	—	100.285(1)	105.96(3)	88.690(4)	—	—
β/deg	97.751(2)	92.764(1)	104.60(3	80.492(4)	96.789(4)	109.939(2)
γ/deg	—	110.054(1)	90.49(3)	78.645(3)	—	—
V/Å^3	3321.5(7)	2562.9(1)	1186.1(4)	1963.7(7)	2024.2(9)	2979.5(9)
Z	4	2	1	2	2	4
d_{calc}/g cm^{-3}	1.763	1.596	1.596	1.647	1.584	1.771
μ/mm^{-1}	1.401	0.94	1.005	1.197	1.161	1.55
θ-Scan range/deg	1.97—23.33	1.79—26.37	1.96—23.41	2.02—23.38	2.14—23.27	2.12—23.31
I_{hkl} measured/independent	25303/4802	18713/10266	8974/3434	15305/5660	5241/2837	10942/2143
R_{int}	0.1124	0.0158	0.0881	0.0807	0.0538	0.0642
Refined parameters	478	759	325	613	316	209
GOOF	0.965	1.002	1.009	0.923	0.952	1.09
R_1	0.049	0.0356	0.0595	0.0456	0.0476	0.0385
wR_2 по $I > 2\sigma(I)$	0.1292	0.1037	0.1401	0.0937	0.1011	0.1132
R_1	0.066	0.432	0.081	0.0672	0.0679	0.0442
wR_2 (based on all data)	0.1232	0.1085	0.1507	0.1005	0.1084	0.1173

X-ray diffraction study. Single-crystal X-ray diffraction data sets were collected on a Bruker AXS SMART APEX CCD diffractometer (Mo-Kα, λ = 0.71073 Å, graphite monochromator, absorption corrections were applied using the Bruker SADABS software, version 2.10). The structures were solved by direct methods and refined by the full-matrix least-squares method with anisotropic displacement parameters for all nonhydrogen atoms. Some H atoms were located in difference electron densi-

Table 4. Crystallographic parameters and the X-ray diffraction data collection and refinement statistics for compounds **12—16**

Parameter	**12**	**13**·EtOH	**14**	**14a**	**15**	**16**
Molecular weight	1234.83	1337.00	948.50	948.50	976.54	1675.28
T/K	218	295	200	295	240	240
Space group	$P\bar{1}$	$I4_1/acd$	$P\bar{1}$	$P\bar{1}$	$P2_1/c$	$P\bar{1}$
a/Å	10.584(5)	25.2059(14)	11.174(2)	11.378(2)	11.193(3)	11.678(3)
b/Å	11.401(6)	—	13.349(2)	13.361(2)	14.738(4)	13.189(3)
c/Å	11.422(6)	41.931(6)	14.091(2)	14.260(2)	13.136(4)	14.105(3)
α/deg	80.763(12)	—	93.023(3)	93.102(3)	—	92.942(3)
β/deg	85.906(10)	—	90.480(3)	90.353(3)	108.471(5)	103.654(3)
γ/deg	79.919(10)	—	110.372(2)	110.378(2)	—	115.014(3)
V/Å^3	1338.1(11)	26640(4)	1966.8(6)	2028.4(5)	2055.4(10)	1884.5(7)
Z	1	16	2	2	4	1
d_{calc}/g cm^{-3}	1.532	1.333	1.602	1.553	1.578	1.476
μ/mm^{-1}	0.582	0.474	0.755	0.732	0.725	0.438
θ-Scan range/deg	1.81—26.59	1.87—25.69	1.94—26.48	1.43—26.47	1.92—26.43	1.73—26.45
I_{hkl} measured/independent	11883/5493	87029/6332	19936/8044	20519/8291	13176/4194	18901/7704
R_{int}	0.1526	0.1124	0.0806	0.0800	0.0799	0.0816
Refined parameters	352	435	604	604	271	511
GOOF	1.041	1.032	0.947	0.848	0.942	1.026
R_1	0.0981	0.0501	0.0524	0.0510	0.0541	0.0554
wR_2 based on reflections with $I > 2\sigma(I)$	0.1472	0.1261	0.0957	0.0915	0.1308	0.1444
R_1	0.1969	0.1246	0.0826	0.0938	0.0777	0.0703
wR_2 (based on all data)	0.1825	0.1699	0.1046	0.1022	0.1405	0.1560

ty maps, and the other hydrogen atoms were positioned geometrically. The H atoms were refined isotropically using the rigid-group approximation. All calculations associated with the structure solution and refinement were carried out with the use of the Bruker SHELXTL software (Version 6.14). Selected bond lengths and bond angles are listed in Table 1. Crystallographic parameters and the X-ray diffraction data collection and refinement statistics are given in Tables 2—4.

Microanalysis of the compounds was carried out on a Carlo Erba 1106 analyzer in the N. N. Vorozhtsov Novosibirsk Institute of Organic Chemistry of the Siberian Branch of the Russian Academy of Sciences.

Magnetic properties of the complexes were measured on a SQUID magnetometer in the temperature range of 5—300 K and a magnetic field of 5 kOe. The paramagnetic terms of the magnetic susceptibility χ were evaluated taking into account the diamagnetic contribution, which was estimated from the Pascal constants. The effective magnetic moment was calculated by the equation

$$\mu_{eff} = \left(\frac{3k}{N_A \beta^2} \cdot \chi T \right)^{1/2} \approx (8\chi T)^{1/2},$$

where N_A is Avogadro´s number, β is the Bohr magneton, and k is the Boltzmann constant. The correction for the temperature-independent paramagnetism was not applied.

This study was financially supported by the Russian Foundation for Basic Research (Project Nos 09-03-00091, 08-03-00025, and 09-03-12108), the Presidium of the Russian Academy of Sciences, the Division of Chemistry and Materials Science of the Russian Academy of Sciences, and the Ural and Siberian Branches of the Russian Academy of Sciences.

References

1. A. Caneschi, D. Gatteschi, P. Rey, *Progr. Inorg. Chem.*, 1991, **39**, 331.
2. V. I. Ovcharenko, R. Z. Sagdeev, *Usp. Khim.*, 1999, **68**, 381 [*Russ Chem. Rev.* (*Engl. Transl.*), 1999, **68**].
3. P. Rey, V. I. Ovcharenko, *Spin Transition Phenomena*, in *Magnetism: Molecules to Materials IV*, Eds. J. S. Miller, M. Drillon, Wiley-VCH, Weinheim, 2003, 41.
4. V. I. Ovcharenko, K. Yu. Maryunina, S. V. Fokin, E. V. Tret´yakov, G. V. Romanenko, V. N. Ikorskii, *Izv. Akad. Nauk, Ser. Khim.*, 2004, 2304 [*Russ. Chem. Bull., Int. Ed.*, 2004, **53**, 2406].
5. F. Lanfranc de Panthou, E. Belorizky, R. Calemczuk, D. Luneau, C. Marcenat, E. Ressouche, P. Turek, P. Rey, *J. Am. Chem. Soc.*, 1995, **117,** 11247.
6. F. Lanfranc de Panthou, D. Luneau, R. Musin, L. Öhrström, A. Grand, P. Turek, P. Rey, *Inorg. Chem.*, 1996, **35**, 3484.
7. F. Iwahory, K. Inoue, H. Iwamura, *Mol. Cryst. Liq. Cryst.*, 1999, **334**, 533.
8. A. Caneschi, P. Chiesi, L. David, F. Ferraro, D. Gatteschi, R. Sessoli, *Inorg. Chem.*, 1993, **32**, 1445.
9. V. I. Ovcharenko, S. V. Fokin, G. V. Romanenko, Yu. G. Shvedenkov, V. N. Ikorskii, E. V. Tret´yakov, S. F. Vasilevskii, *Zh. Strukt. Khim.*, 2002, **43**, 163 [*Russ. J. Struct. Chem.* (*Engl. Transl.*), 2002, **43**, 153].
10. V. I. Ovcharenko, S. V. Fokin, G. V. Romanenko, V. N. Ikorskii, E. V. Tretyakov, S. F. Vasilevsky, R. Z. Sagdeev, *Mol. Phys.*, 2002, **100**, 1107.
11. M. Baskett, P. M. Lahti, A. Paduan-Filho, N. F. Oliveira, Jr. *Inorg. Chem.*, 2005, **44**, 6725.
12. M. Fedin, S. Veber, I. Gromov, V. Ovcharenko, R. Sagdeev, E. Bagryanskaya, *J. Phys. Chem. A*, 2007, **111**, 4449.
13. M. Fedin, S. Veber, I. Gromov, K. Maryunina, S. Fokin, G. Romanenko, R. Sagdeev, V. Ovcharenko, E. Bagryanskaya, *Inorg. Chem.*, 2007, **46**, 11405.
14. M. Fedin, S. Veber, I. Gromov, V. Ovcharenko, R. Sagdeev, A. Schweiger, E. Bagryanskaya, *J. Phys. Chem. A*, 2006, **110**, 2315.
15. S. L. Veber, M. V. Fedin, A. I. Potapov, K. Yu. Maryunina, G. V. Romanenko, R. Z. Sagdeev, V. I. Ovcharenko, D. Goldfarb, E. G. Bagryanskaya, *J. Am. Chem. Soc.*, 2008, **130**, 2444.
16. V. I. Ovcharenko, G. V. Romanenko, K. Y. Maryunina, A. S. Bogomyakov, E. V. Gorelik, *Inorg. Chem.*, 2008, **47**, 9537.
17. M. Fedin, V. Ovcharenko, R. Sagdeev, E. Reijerse, W. Lubitz, E. Bagryanskaya, *Angew. Chem., Int. Ed.*, 2008, **47**, 6897.
18. V. I. Ovcharenko, S. V. Fokin, G. V. Romanenko, V. N. Ikorskii, D. S. Yachevskii, D. L. Chizhov, V. N. Charushin, *Izv. Akad. Nauk, Ser. Khim.*, 2006, 1836 [*Russ. Chem. Bull., Int. Ed.*, 2006, **55**, 1904].
19. J. W. Guthrie, R. L. Lintvedt, M. D. Glick, *Inorg. Chem.*, 1980, **19**, 2949.
20. B. Bleaney, K. D. Bowers, *Proc. Roy. Soc. A*, 1952, **214**, 451.
21. D. S. Yachevskii, D. L. Chizhov, V. G. Ratner, K. I. Pashkevich, *Izv. Akad. Nauk, Ser. Khim.*, 2001, 1176 [*Russ. Chem. Bull., Int. Ed.*, 2001, **50**, 1233].

Received June 18, 2009;
in revised form March 25, 2010